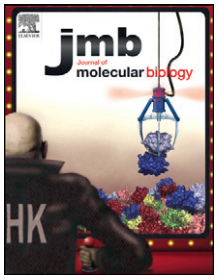

Semi-Empirical Structure Determination of *Escherichia coli* Hsp33 and Identification of Dynamic Regulatory Elements for the Activation Process

Yoo-Sup Lee[1,2], Jinhyuk Lee[3,4,8], Kyoung-Seok Ryu[5], Yuno Lee[6], Tai-Geun Jung[1,9], Jeong-Hwa Jang[1], Dae-Won Sim[1], Eun-Hee Kim[5], Min-Duk Seo[2,7], Keun Woo Lee[6] and Hyung-Sik Won[1]

*1 - **Department of Biotechnology,** Research Institute (RIBHS) and College of Biomedical and Health Science, Konkuk University, Chungju, Chungbuk 27478, Republic of Korea*
*2 - **Department of Molecular Science and Technology,** Ajou University, Suwon, Gyeonggi 16499, Republic of Korea*
*3 - **Korean Bioinformation Center,** Korea Research Institute of Bioscience and Biotechnology, Daejeon 34141, Republic of Korea*
*4 - **Department of Bioinformatics,** University of Sciences and Technology, Daejeon 34113, Republic of Korea*
*5 - **Protein Structure Group,** Korea Basic Science Institute, 162 Yeongudanji-ro, Ochang, Chungbuk 28119, Republic of Korea*
*6 - **Division of Applied Life Science (BK21 Plus Program),** Systems and Synthetic Agrobiotech Center, Plant Molecular Biology and Biotechnology Research Center, Research Institute of Natural Science, Gyeongsang National University, Jinju 52828, Republic of Korea*
*7 - **College of Pharmacy,** Ajou University, Suwon, Gyeonggi 16499, Republic of Korea*

***Correspondence to Hyung-Sik Won:** Department of Biotechnology, Konkuk University, 268 Chungwon-daero, Chungju, Chungbuk 27478, Republic of Korea. wonhs@kku.ac.kr*
http://dx.doi.org/10.1016/j.jmb.2015.09.029
Edited by R. W. Kriwacki

Abstract

The activation process of the redox-regulated chaperone heat shock protein 33 (Hsp33) is constituted by the oxidation-induced unfolding of the C-terminal zinc-binding domain and concomitant oligomerization of the N-terminal core domain. Herein, the semi-empirical solution structure of *Escherichia coli* Hsp33 in the reduced, inactive form was generated through conformational space annealing calculations, utilizing minimalistic NMR data and multiple homology restraints. The various conformations of oxidized Hsp33 and some mutant forms were also investigated in solution. Interestingly, a specific region concentrated around the interdomain linker stretch and its interacting counterparts, the N-terminal β-strand 1 and α-helix 1, hardly showed up as signals in the NMR measurements. The NMR spectra of an Hsp33 derivative with a six-residue deletion in the disordered N-terminus implied a plausible conformational exchange associated with the identified region, and the corresponding exchange rate appeared slower than that of the wild type. Subsequent mutations that destroyed the structure of the β1 or α1 elements resulted in the formation of a reduced but active monomer, without the unfolding of the zinc-binding domain. Collectively, structural insights into the inactive and active conformations, including wild-type and mutant proteins, suggest that the dynamic interactions of the N-terminal segments with their contacting counterpart, the interdomain linker stretch, in the reduced, inactive state are the structural determinants regulating the activation process of the post-translationally regulated chaperone, Hsp33.

© 2015 Elsevier Ltd. All rights reserved.

Introduction

As denaturation of cellular macromolecules by heat stress can prove fatal to cells, heat shock proteins are expressed to serve as molecular chaperones. Heat shock protein 33 (Hsp33), a prokaryotic molecular chaperone, is distinguished from the majority of general heat shock proteins by its capability to cope with oxidative heat conditions and/or severe, acute oxidative stress [1,2]. The activated Hsp33 protects cells from the conditions of stress by functioning as a holdase that binds the folding intermediates of substrate proteins to prevent their ultimate, irreversible denaturation. In particular, Hsp33 has been verified as an essential chaperone for bacteria in the resistance against

bleach treatment [3,4]. Additionally, it is also responsible for bacterial tolerance to solvent stress [5] and the inhibition of the bacterial functional amyloid assembly [6]. Moreover, involvement of Hsp33 in an essential chaperone network was recently suggested to have a key, housekeeping role in the absence of exogenous stressors [7].

The Hsp33 structure can be divided into the following four functional parts (Fig. 1): the N-terminal core domain (NCD; residues 1–178) constituting the dimerization interface, the middle linker domain (MLD; residues 179–216) consisting of three α-helices (α5–α7), an extended stretch (residues 217–231) with interdomain linker strands (β10–β11), and the C-terminal regulatory domain (CRD; residues 232–294, which is also called the "redox-switch domain") responsible for zinc binding. As a holdase chaperone, the functional cycle of Hsp33 is thought to be very sophisticated, comprising at least six different conformations. They are referred to herein as ^{R}Hsp33^{M}, ^{hO}Hsp33^{M}, ^{O}Hsp33^{M}, ^{O}Hsp33^{D}, ^{O}Hsp33^{O}, and ^{R}Hsp33^{D}. Under non-stressed conditions, Hsp33 behaves as an inactive, reduced monomer (^{R}Hsp33^{M}) that binds a single zinc ion, which is coordinated by the thiolate groups of four conserved cysteines (C232, C234, C265, and C268) at the CRD [8]. The activation process is triggered by oxidation of the conserved cysteines, leading to the dissociation of zinc and concomitant unfolding of the CRD [9,10]. Four types of oxidized Hsp33 have previously been observed *in vitro* [10–13]. First, the half-oxidized monomer (^{hO}Hsp33^{M}), which was suggested to be inactive [11] or only partially active upon limited substrates [9,12–15], possesses just one disulfide bond formed by two of the four conserved cysteines (C265 and C268). Then, the fully oxidized dimer (^{O}Hsp33^{D}), which contains two intramolecular disulfide bonds within the four conserved cysteines (C265–C268 and C232–C234) in each monomer, has been regarded as the functional unit, exerting an entire activity to bind substrates [11]. However, a monomeric form with both of the two disulfide bonds has also been suggested as an active species [10]. Finally, the higher-order oligomers of oxidized Hsp33 (^{O}Hsp33^{O}) were previously identified as more potent forms, and it was suggested that they were more favored than ^{O}Hsp33^{D} *in vivo* [13]. Substrate dissociation from the active, oxidized Hsp33 cannot be achieved solely by reduction, as the DnaK/DnaJ/GrpE foldase system is also required *in vivo*. Reduction of the substrate-bound ^{O}Hsp33^{D} without a linkage to the foldase system leads to the formation of a reduced Hsp33 dimer (^{R}Hsp33^{D}), a reduced but active species, which is still bound to its substrates [16,17].

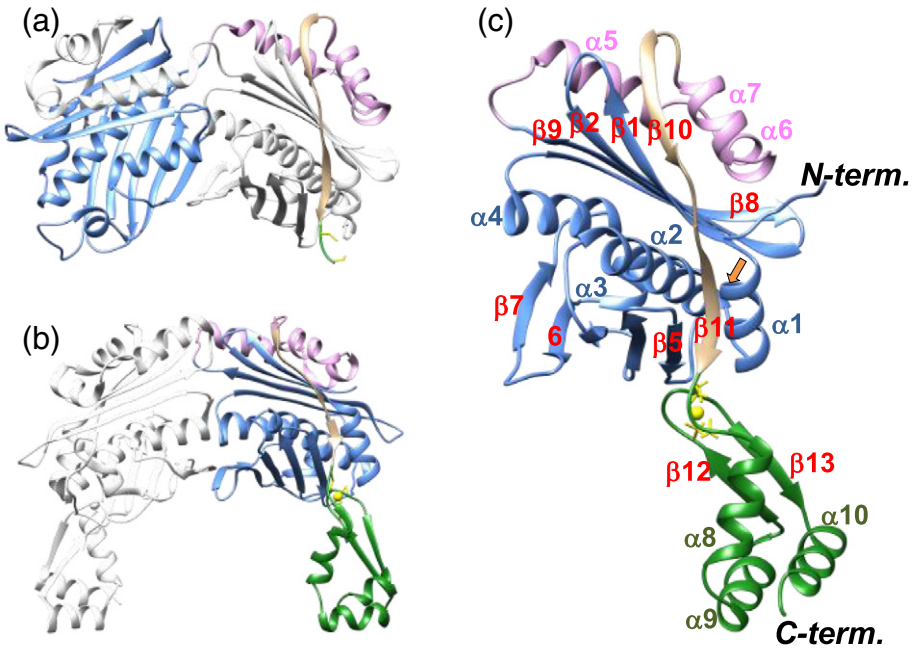

Fig. 1. Structural representations of Hsp33. Each domain of the polypeptide chain is colored blue, pink, tan, and green, representing the NCD, MLD, interdomain linker stretch, and CRD, respectively. (a) Crystal structure of the ΔC-*Ec*Hsp33 dimer (PDB entry 1HW7), where the CRD was truncated during crystallization [21,22]. (b) Crystal structure of the dimeric *Bs*^{R}Hsp33 (PDB entry 1VZY). (c) The present semi-empirical model structure of *Ec*^{R}Hsp33^{M}. Secondary structural elements are labeled including the 10 α-helices and the 13 β-strands with the arrangement of N-ββααββββαββαββααααββααββα-C. The bound zinc ion (sphere) and the conserved Cys side chains are depicted in yellow. The position of the L30 for mutagenesis is indicated by an orange arrow. The structural figures were generated, using the UCSF Chimera program [39].

Hsp33 has been evaluated as an ideal molecule for an in-depth analysis of the structural mechanisms of chaperones [18], and its activation process is a greatly intriguing subject, as it needs to lose its structure to gain function [19,20]. A number of crystal structures [14,17,21–23] are available for Hsp33, and recent achievements by Reichmann *et al.* have provided structural insights into how the activated Hsp33 can recognize and deliver the unfolding substrates to other foldase chaperones [19]. Nonetheless, a detailed structural basis of the activation process, which is accompanied by dramatic alterations of the conformation and oligomeric state, has been so far obscure, particularly due to limitations of the known crystal structures and doubtful physiological relevance [12]. In this study, NMR study was conducted to characterize the various Hsp33 conformations in solution and to address a plausible dynamic fluctuation of the protein that appears critical for the regulation of the activation process.

Results

NMR assignments and semi-empirical structure determination of the reduced species

The resonances from the full-length (1–294) Hsp33 in its inactive, reduced monomer state (^{R}Hsp33^{M}) were well resolved in the whole region of the measured NMR spectra (Fig. 2a), supporting its well-ordered conformation. In our previous approach to the backbone NMR assignments of ^{R}Hsp33^{M}, the experimental conditions of 298 K and pH 7.4 were employed [12,24] for which the isolated CRD structure has been determined [8]. In the present work, the assignments were complemented (Supplementary Discussion) by a comparative analysis of the additional triple-resonance data sets that were obtained at a higher temperature (313 K) and at two different pH levels (7.4 and 6.5), enabling a secondary structure

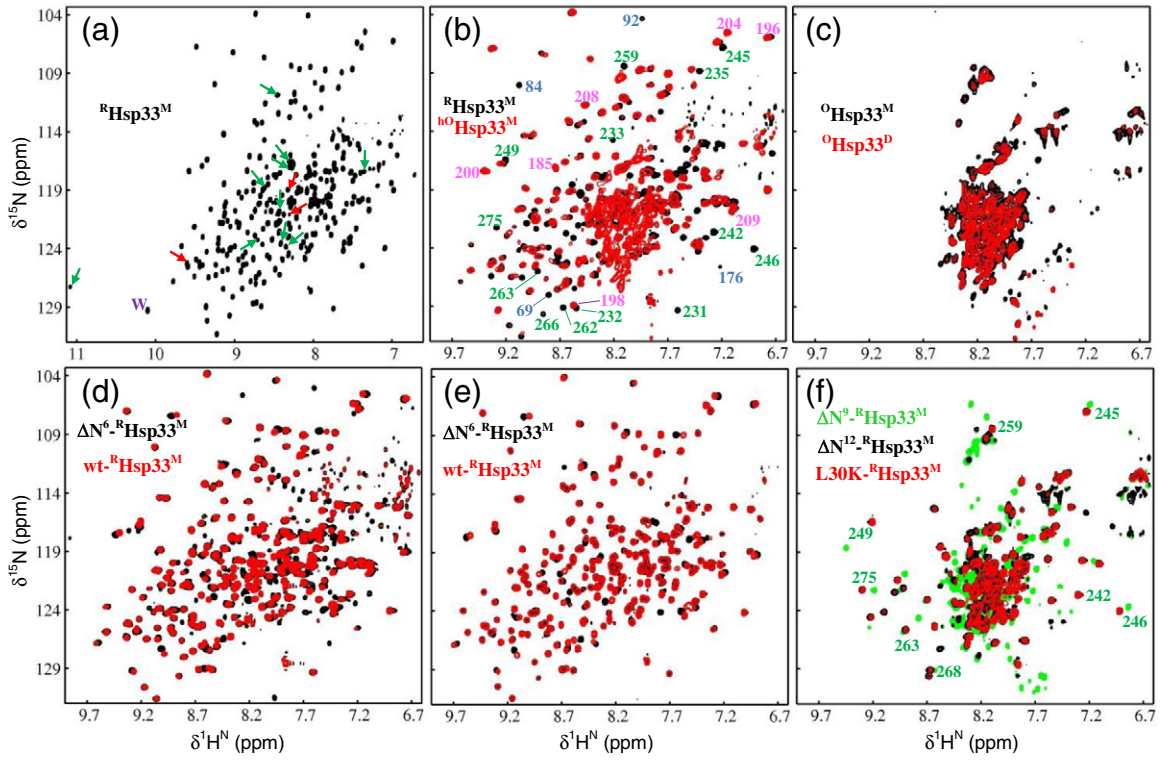

Fig. 2. Structural perturbation of Hsp33 monitored by the 2D [^{1}H/^{15}N]TROSY spectra. (a) Representative spectrum of ^{R}Hsp33^{M} measured at 313 K. The 13 resonances that were not detected at 298 K are indicated by arrows. Three of them, distinguished by red arrows, could not be assigned due to the absence of sequential connectivity. For clarity, the spectra in (b) to (f) were enlarged in the up-field region of the single Trp side-chain peak [marked by "W" in (a)]. (b and c) Spectral changes depending on redox status. The spectra of ^{R}Hsp33^{M}, ^{hO}Hsp33^{M}, ^{O}Hsp33^{M}, and ^{O}Hsp33^{D}, measured at 298 K, were superimposed. (d and e) Spectral comparison between wild-type ^{R}Hsp33^{M} and ΔN^{6}-^{R}Hsp33^{M}, at 298 K (d) and 313 K (e). (f) Spectral superimposition of the reduced, active mutants. In the well-resolved regions in (b) and (f), indicator peaks for the NCD, MLD, and CRD are labeled with corresponding residue numbers colored blue, pink, and green, respectively. The spectrum in (a) was measured for [^{13}C/^{15}N/^{2}H]Hsp33, while all other spectra were obtained with [^{15}N]Hsp33 proteins.

determination [25-27] of the ^{R}Hsp33^{M} through use of the secondary chemical shifts and TALOS+ prediction (Fig. 3). The $^{1}H^{N}/^{1}H^{N}$ nuclear Overhauser enhancements (NOEs) observed in the 3D [^{15}N]edited NOE spectroscopy (NOESY) spectra were also used to supplement the secondary structure determination and to deduce the β-sheet topology. Meanwhile, distance restraints for the 3D structure calculations were limited to those between amide protons, as the NOESY spectra were obtained with deuterated samples, making the resonance assignments unavailable for side-chain protons. As can be seen in Fig. 3, however, the determined secondary structure arrangements (position and length of each secondary structure element and the β-sheet topology) of ^{R}Hsp33^{M} showed a remarkable

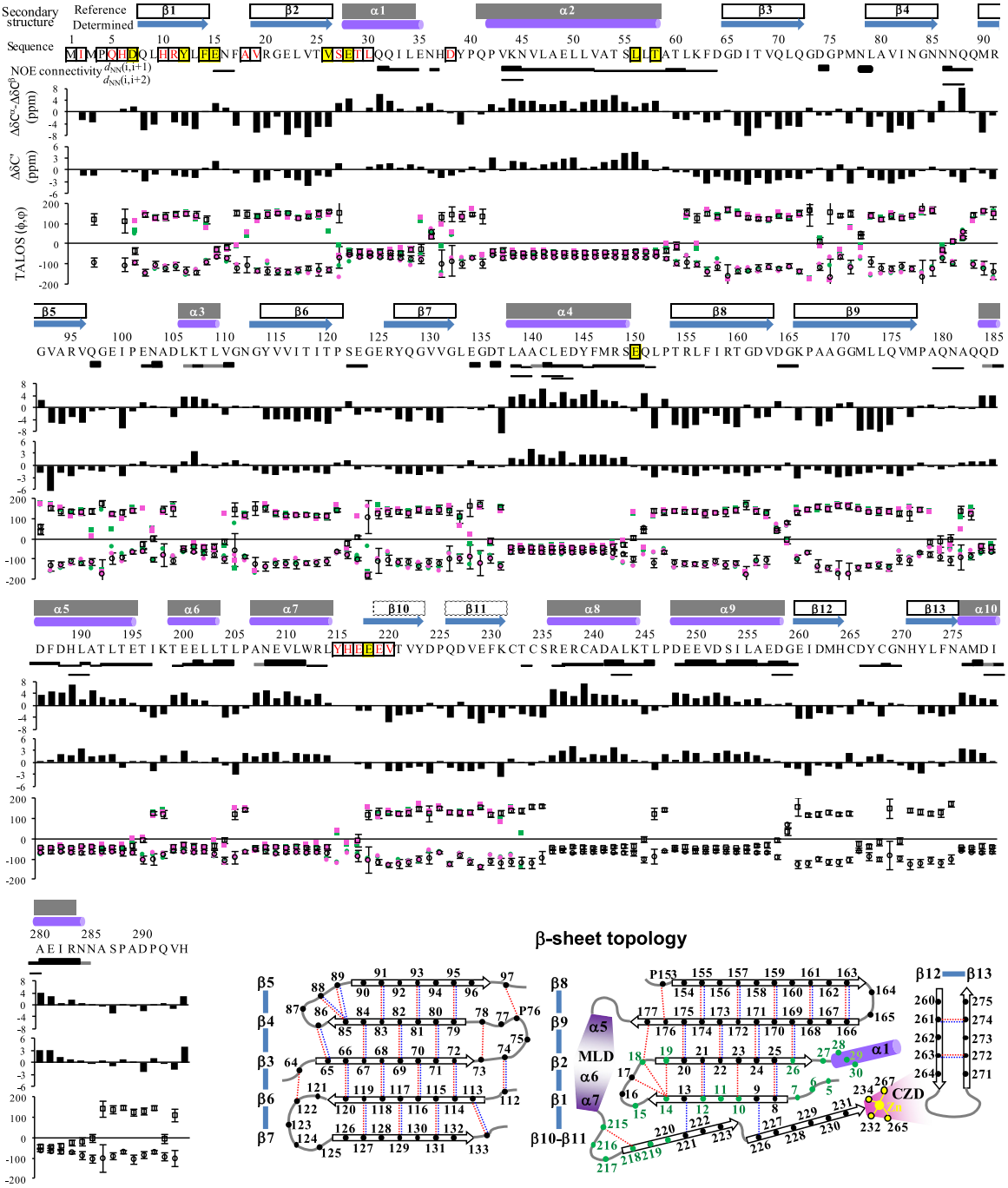

Fig. 3 (*legend on next page*)

consistency with those expected from the combination of the isolated CRD and ΔC-Hsp33 structures [8,21,22]. Additionally, the secondary structure of Hsp33 appeared to be conserved between the bacterial species (Supplementary Fig. S1), and we have previously shown that the interdomain contact site of ^{R}Hsp33^{M} in solution corresponded with that observed in the crystal structure of ^{R}Hsp33^{D} (Fig. 1b) [12]. Based on the structural similarities, the recently developed hybrid modeling strategy [28] could therefore be employed as a promising method to overcome the insufficient experimental restraints and to generate a reliable, semi-empirical structure of ^{R}Hsp33^{M} with minimalistic NMR restraints, supplemented by multiple homology restraints (Supplementary Methods). In particular, a well-converged structure ensemble with little violation of the empirical restraints (Supplementary Table 1) could be successfully generated by the conformational space annealing (CSA) calculation [29]. Finally, the energy-minimized average structure, after a final refinement via a molecular dynamics simulation in an explicit water model, is presented in Fig. 1c as a sound-quality (Supplementary Table 1) model for structural inspection.

Isolation and structural characterization of the oxidized species

Intriguingly, a gel-filtration analysis of the oxidized Hsp33 solution detected four distinguished species (Fig. 4a), while only three of the oxidized-form types were previously identified. As can be seen in Fig. 4a, the latest elution, marked with an apparent molecular mass (M_r^{app}) of 43 kDa, and the largest species ($M_r^{app} > 95$ kDa) eluted from the column void volume (43 ml) could easily be assigned as the known ^{hO}Hsp33^{M} and ^{O}Hsp33^{O} species, respectively, as previously identified [11–13]. Surprisingly, the distinguished elution at an M_r^{app} of 70 kDa, seen in Fig. 4a (71 kDa in Fig. 4b after isolation), contained a single species with an actual molecular mass of approximately 32 kDa, which was estimated by multi-angle light scattering (MALS) analysis (Supplementary Fig. S2a). Meanwhile, the oxidized species in the second eluent ($M_r^{app} \approx 90$ kDa) could be identified as the known ^{O}Hsp33^{D} species, as it showed an actual molecular mass of approximately 66 kDa (Supplementary Fig. S2b). Thus, the oxidized species in the third elution ($M_r^{app} \approx 70$ kDa), which was formerly regarded as a dimer [12], could be newly interpreted as the monomeric ^{O}Hsp33^{M} state. Additionally, we demonstrated that the isolated ^{O}Hsp33^{M} efficiently prevented the aggregation of a substrate protein (Fig. 5), thereby identifying it as the minimal unit of Hsp33 that exerts an entire chaperone activity.

The higher hydrodynamic size (M_r^{app} of 39 kDa; Fig. 4a) that was observed for ^{R}Hsp33^{M}, compared with its actual molecular mass (33 kDa), is attributable to its non-globular shape (Fig. 1c), which generally promotes fast elution in gel filtration. Likewise, the remarkable increment of M_r^{app} of the oxidized species could be attributed to dramatic unfolding at different extents, as evidenced in the far-UV circular dichroism (CD) spectra (Fig. 6 and Supplementary Fig. S3). The 2D [^{1}H/^{15}N]transverse relaxation optimized spectroscopy (TROSY) spectrum of ^{hO}Hsp33^{M} also showed an appreciable collapse in the middle of the spectrum (Fig. 2b), indicating a significant unfolding of the structure. As deduced from the indicator peaks in the well-resolved regions of the ^{hO}Hsp33^{M} spectrum, the resonances from the CRD mostly disappeared, likely due to extreme shifts to the collapsed region, whereas the characteristic resonances from the MLD were still obvious with retention of the same chemical shifts. This observation is partly in support of the structural model for ^{hO}Hsp33^{M} proposed by Ilbert *et al.* [11], which suggested only a partial unfolding that was restricted to the CRD. However, as some resonances from the NCD including the V69, G84, G92, and V176 also disappeared in the ^{hO}Hsp33^{M} spectrum (Fig. 2b), the possibility of additional conformational changes in the NCD could not be excluded. Then, consistent with the CD results, the NMR spectrum of the isolated ^{O}Hsp33^{M}, which was characterized by an enlargement of the collapsed region (Fig. 2c), corroborated

Fig. 3. Determination of secondary structure and β-sheet topology of ^{R}Hsp33^{M}. Determined α-helix and β-strand elements are represented by cylinders and arrows, respectively, along the amino acid sequence. The reference structure was derived from the crystal structure of ΔC-Hsp33 [21,22] and the NMR structure of CRD [8]. β10 and β11 (broken line) were not flagged as β-strands by the DSSP despite the obvious β-like folds [21,22]. In the sequence, the residues with missing assignments (non-detected signals) of the backbone amid resonances at 298 K and pH 7.4 are boxed. Resonance observations made upon increasing the temperature (313 K) are marked by yellow shadows. The residues marked in red showed no signal, even at the higher temperature and lower pH (6.5). The height of the NOE connectivity bars reflects the relative intensity of the correlation, while the gray bars indicate putative assignments due to spectral overlap. Secondary chemical shifts of ^{13}C atoms ($\Delta\delta C^{\alpha}$, $\Delta\delta C^{\beta}$, and $\Delta\delta C'$) are presented as the chemical shift deviations from the random-coil reference values of individual amino acids [27]. The TALOS+ prediction presents the backbone dihedral φ (empty rectangles) and ϕ (empty circles) angles with standard deviations (error bars). The reference φ (filled rectangles) and ϕ (filled circles) angles were extracted from the ΔC-Hsp33 crystal structures (green for PDB entry 1I7F and pink for PDB entry 1HW7). In the inset, the β-sheet topology was deduced from the inter-strand $^{1}H^{N}/^{1}H^{N}$ NOEs (blue dotted lines), in comparison with the inter-strand hydrogen bonding of the known crystal structures (red dotted lines). Residue numbers in green indicate the missing assignments of the amide protons at 298 K.

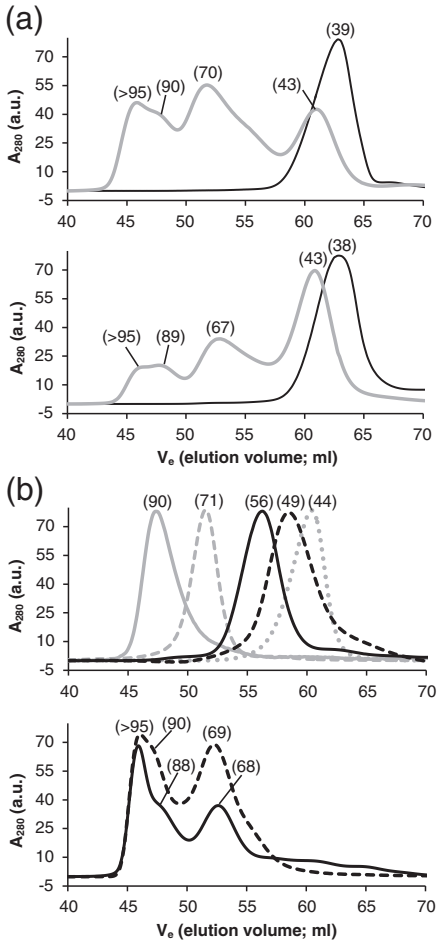

Fig. 4. Hydrodynamic behaviors of the wild-type and mutant Hsp33 species, represented by gel-filtration elution profiles. For convenience of comparison, the *y*-axis values (absorbance at 280 nm; arbitrary unit) were re-scaled to show similar heights for all of the profiles. The hydrodynamic size (kDa) deduced from the elution volume was presented in parenthesis for each distinguishable peak. (a) Comparison between wild type (upper panel) and ΔN^6-Hsp33 (lower panel), before and after oxidation (reduced: black lines; oxidized mixture: gray lines). Individual elution profiles of the three isolated oxidized species of wild-type Hsp33 are shown by gray lines in (b) (continuous, $^{O}Hsp33^{D}$; broken, $^{O}Hsp33^{M}$; dotted, $^{hO}Hsp33^{M}$). (b) Comparison between ΔN^{12}-Hsp33 (black, continuous lines) and L30K-Hsp33 (black, broken lines), before and after oxidation (reduced: upper panel; oxidized mixture: lower panel).

that a more profound unfolding extended to include the MLD. The extremely rare detection of resolved peaks in the $^{O}Hsp33^{M}$ spectrum was attributable to the hybrid conformational feature that accompanied the conjugation of the disordered and ordered regions (Supplementary Discussion). In addition, $^{O}Hsp33^{D}$ and $^{O}Hsp33^{M}$ appeared to share, as a minimum, the same conformation at the secondary structure level, since they showed nearly identical CD (Supplementary Fig. S3) and NMR (Fig. 2c) spectra. Meanwhile, based on the CD spectra (Supplementary Fig. S3), the oligomerization seemed to be accompanied by a further expansion of unfolding compared with $^{O}Hsp33^{D(M)}$.

Identification of dynamic regions

The present NMR results for $^{R}Hsp33^{M}$ contained some missing assignments of backbone amides due to the deficiency of observed signals (Supplementary Discussion). Additionally, 13 resonances including three non-assigned peaks were not detected in the 2D and/or 3D spectra at a lower temperature (Figs. 2a and 3). These results suggested that a significant portion of the residues in the protein hardly showed up as signals in the NMR measurements. Owing to severe line-broadening, signals from dynamic regions such as loops are often invisible in protein NMR when they are under a certain chemical exchange at an intermediate rate in the NMR timescale. However, the missing or faint resonances in the present results are more abundant than what is generally observed for globular proteins. Moreover, the identified regions with the invisible signals included elements of the secondary structure, particularly the β1 and α1 in the N-terminal region and the β10 in the interdomain linker stretch, for which stable folds were obvious in the known crystal structures (Fig. 1). Interestingly, most of the missing assignments were mapped within the following two specifically related sites: the N-terminus (about 30 residues) and a part of the interdomain linker stretch (Y215–T221) (Fig. 3). According to both our model structure and the known crystal structures, these two regions are adjacent to each other with frequent contacts (Fig. 1 and inset in Fig. 3). The convergence of the hardly detected signals into specific regions therefore led us to suppose that peculiar dynamics may be associated with those regions in solution. Then, direct experimental evidence of the unusual dynamics could be derived from the NMR spectra of ΔN^6-Hsp33, an Hsp33 derivative with a six-residue deletion from the N-terminus. Based on our model structure and the known crystal structures, the N-terminal six residues are not involved in the first secondary structure element, β-strand 1 (Q8–F14). Results from the gel-filtration analysis (Fig. 4a) and far-UV CD spectroscopy (Supplementary Fig. S3) indicated no significant change of the overall conformation from the six-residue N-terminal deletion, in both the reduced and the oxidized states. The 2D [$^{1}H/^{15}N$]TROSY spectrum of ΔN^6-$^{R}Hsp33^{M}$, which was quite similar to that of wild-type $^{R}Hsp33^{M}$, also supported the conformational consistency (Fig. 2d and e). Interestingly, however, ΔN^6-$^{R}Hsp33^{M}$ showed a lot more NMR signals at 298 K (Fig. 2d) than the wild-type

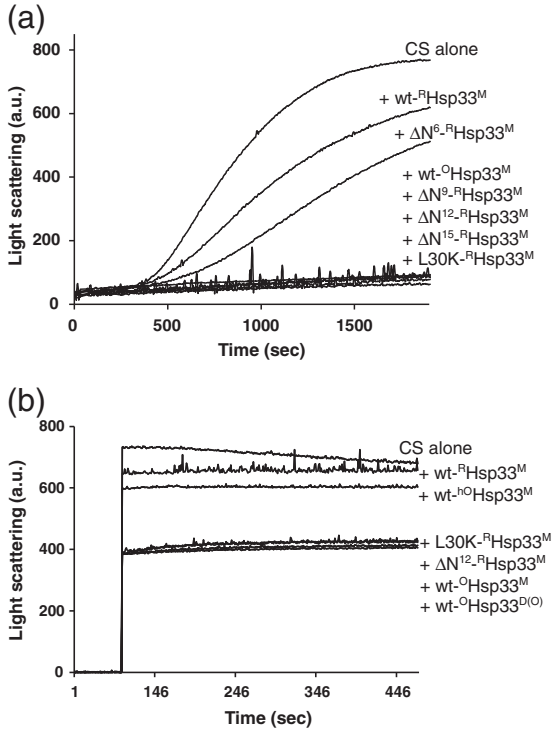

Fig. 5. Holdase activities of the wild-type and mutant Hsp33 proteins. (a) Light scattering (arbitrary unit) upon thermal aggregation of CS (88 nM) is plotted along the incubation time at 43 °C, in the absence of added protein (CS alone) and in the presence of 0.4 μM (4.5-fold molar excess) of wild-type ^{R}Hsp33^{M}, wild-type ^{O}Hsp33^{M}, ΔN^{6}-^{R}Hsp33^{M}, ΔN^{9}-^{R}Hsp33^{M}, ΔN^{12}-^{R}Hsp33^{M}, ΔN^{15}-^{R}Hsp33^{M}, and L30K-^{R}Hsp33^{M}, respectively. (b) Light scattering (arbitrary unit) upon chemical aggregation of CS (75 nM) is plotted along the incubation time at 30 °C, in the absence of Hsp33 (CS alone) and in the presence of 375 nM (5-fold molar excess) of wild-type [^{R}Hsp33^{M}, ^{hO}Hsp33^{M}, ^{O}Hsp33^{M}, and ^{O}Hsp33$^{D(O)}$] and mutant (ΔN^{12}-^{R}Hsp33^{M} and L30K-^{R}Hsp33^{M}) Hsp33 species, respectively.

^{R}Hsp33^{M} despite containing a lower number of amino acids. It is also noteworthy that the number of newly appearing peaks in the ΔN^{6}-^{R}Hsp33^{M} spectrum was somewhat higher than the number of non-assigned residues. In addition, all of the new peaks disappeared at a higher temperature of 313 K (Fig. 2e), while they were intensified at a lower temperature of 283 K (data not shown). One of the most plausible explanations for this extraordinary spectral change could be derived from a different contribution of molecular dynamics associated with the N-terminus. It is likely that, in the wild-type ^{R}Hsp33^{M}, the regions identified to have missing assignments undergo a certain conformational exchange at an intermediate rate on the NMR timescale, which broadened the corresponding resonances. Then, elevating the temperature could increase the exchange rate to allow the detection of some of the signals. In contrast, in ΔN^{6}-^{R}Hsp33^{M}, the exchange rate could be slowed down by the six-residue N-terminal deletion, making the signals visible with doubled peaks, reflecting both conformations under equilibrium. Then, at higher temperatures, the exchange rate would be accelerated again to an intermediate timescale, thereby severely broadening the exchanging signals again. In summary, we could postulate that the pair of the interdomain linker stretch and the N-terminal stretch in ^{R}Hsp33^{M} in solution would be under a dynamic conformational equilibrium, leading to unstable or transient interactions between the two stretches. We therefore performed the following mutagenesis, intrigued by the functional implications of the putatively dynamic regions.

Generation and structural characterization of reduced, active mutants

Mutations were introduced at dynamic regions in the N-terminal β1 and α1 for the identification of novel regulatory elements. We first generated three

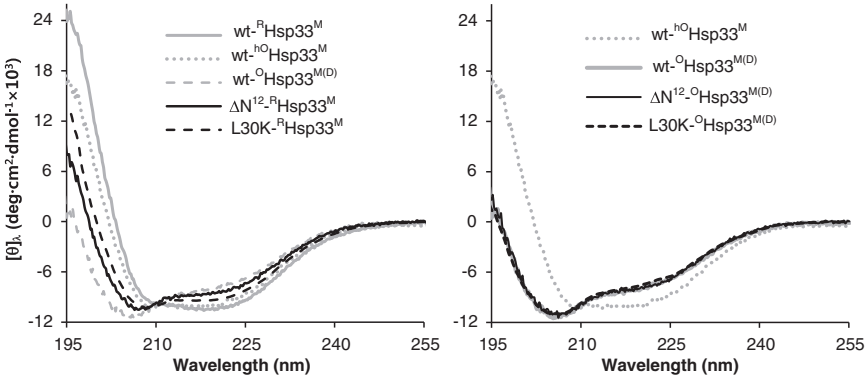

Fig. 6. Oxidation-induced conformational changes of the β1/α1-defective mutants. Far-UV CD spectra of ΔN^{12}-Hsp33 (black, continuous lines) and L30K-Hsp33 (black, broken lines), before and after oxidation (reduced: left panel; oxidized mixture: right panel) are presented in comparison with the individual spectra of the wild-type species isolated in the reduced and oxidized states (gray lines).

kinds of N-terminal deletion mutants ΔN^{9}-, ΔN^{12}-, and ΔN^{15}-^{R}Hsp33, in addition to the ΔN^{6}-^{R}Hsp33^{M}, to disrupt (ΔN^{9}- and ΔN^{12}-Hsp33) or completely delete (ΔN^{15}-Hsp33) the β1 (Q8–F14) strand, which is adjacent on the N-terminal part (β10) of the interdomain linker stretch (Fig. 1). As the behavior of all three of the mutant proteins was nearly identical (Supplementary Fig. S4), only the results obtained with ΔN^{12}-Hsp33 are interpreted here. Despite their monomeric state, which was confirmed by a MALS analysis (Supplementary Fig. S2c), the reduced β1-defective mutants were detected at a quite lower elution volume in the gel-filtration analysis (Fig. 4b) compared with the wild-type ^{R}Hsp33^{M} elution (Fig. 4a). The CD (Fig. 6a) and NMR spectra indicated that this extraordinary behavior was due to the unique conformation with remarkable unfolding. In particular, the NMR spectra (Fig. 2f) identified MLD as one of the unfolding sites, for which signals were not detected in the well-resolved spectral regions. In contrast, the indicator peaks of folded CRD were clearly observed, albeit at exceptionally shifted positions for ΔN^{9}-^{R}Hsp33, which certified the reduced, zinc-bound state of the CRD. Finally, clear chaperone activity was observed for the reduced forms of the β1-defective mutants (Fig. 5). It is known that a 4–5 molar excess of oxidized wild-type Hsp33 is sufficient to almost completely suppress the thermal aggregation of the experimental client protein, citrate synthase (CS) [1,11,30]. The efficacy and potency of the *in vitro* chaperone activity for the reduced, β1-defective mutants appeared comparable to those of the active, oxidized wild-type Hsp33, in both the thermal and the chemical aggregations assays (Fig. 5 and Supplementary Fig. S5). We therefore concluded that breaking the dynamic β1 interactions with the interdomain linker stretch, even without oxidation and CRD unfolding, resulted in a critical unfolding of the MLD that accorded chaperone activity.

Among the three non-visible positions (E28–L30) in the α1 by NMR (Fig. 3), position 30 is conserved with hydrophobic amino acids among Hsp33 proteins from different bacterial species [8,21,22] (Supplementary Fig. 1). We thus substituted the leucine with the charged amino acid lysine to confer polarity without reducing the bulky side chain. Notably, the conformational behavior of the L30K-^{R}Hsp33 was quite similar to those of the β1-defective mutants (Figs. 2f, 4b, and 6) and nearly identical with the behavior of Y12E-^{R}Hsp33 (Supplementary Fig. S6), which was previously identified by Cremers *et al.* [30] as a constitutively active monomer form. The L30K-^{R}Hsp33^{M} also showed appreciable unfolding (Fig. 6), with retaining the folded CRD (Fig. 2f). Finally, as the L30K-^{R}Hsp33^{M} also exhibited clear chaperone activity with similar efficacy and potency to those of the ΔN^{12}-^{R}Hsp33 (Fig. 5 and Supplementary Fig. S5), it was identified as another active species with intrinsically unfolded MLD (Fig. 2f). Based on the structural model in Fig. 1, the α1 helix is anticipated to make frequent contact with the C-terminal part (β11) of the interdomain linker stretch. Although the L30 residue does not have direct contact with the interdomain linker stretch, it can be postulated that the mutation of the conserved L30 residue would destroy the helix conformation of α1, causing subsequent defects in its cooperative interaction with the interdomain linker stretch. The results therefore suggest that the α1 element, in addition to β1, is also critically involved in regulating the chaperone activity of Hsp33.

The gel-filtration results (Fig. 4b) and CD (Fig. 6) results implied that the extent of unfolding of L30K-^{R}Hsp33^{M} was slightly less than that of ΔN^{12}-^{R}Hsp33^{M}. However, both ΔN^{12}- and L30K-Hsp33 showed common hydrodynamic behavior (Fig. 4) consistent with that of the wild type after oxidation, except that they could not produce the half-oxidized monomer species. In addition, the β1/α1-defective mutants (represented by ΔN^{12}- and L30K-Hsp33) were further unfolded upon oxidation, likely due to the oxidation-induced CRD unfolding, and the CD spectra of their oxidized forms appeared nearly identical with the oxidized wild-type spectra (Fig. 6).

Discussion

Hsp33 is an interesting molecule that is subject to massive conformational rearrangements including a significant unfolding and the increased exposure of hydrophobic surfaces for its functional activation [18–20,31]. However, none of the known crystal structures could conclusively identify the exact fold of the inactive, reduced Hsp33 monomer form (^{R}Hsp33^{M}) [12]. The present work provided a reliable structure of ^{R}Hsp33^{M} in solution by establishing an advanced approach to semi-empirical structural modeling using the CSA method. In addition, the various conformations of oxidized Hsp33 were also characterized in solution by NMR, thereby providing structural insights into the activation process.

Hsp33 contains two domains, CRD and MLD, which unfold for structural activation [3,11,19,30]. Accordingly, both domains, for which the known crystal structures commonly showed relatively high *B*-factors implying flexible properties [17,21,22], appear to adopt intrinsically unstable folds that are prone to unfolding. For example, the hydrophobic core of the CRD is not favorable to provide a stable structure [8]. The MLD is also not tightly folded, and it shows conformational differences between the two subunits in the asymmetric unit of the ΔC-Hsp33^{D} crystal structures [21,22]. The inactive ^{R}Hsp33^{M} should therefore possess certain elements that are capable of stabilizing the folded conformations of the CRD and MLD. For the CRD, the tightly ($K_d < 10^{-17}$ M) [32] bound zinc ion is certainly the

key factor that maintains the folded conformation, as the release of zinc, even without the disulfide bond formation of cysteines, is sufficient for its unfolding [8,9]. Likewise, the MLD interacts with the NCD to maintain its folded state [21]. However, the N-terminal end (P178) of the MLD is liable to flip [17] (refer to Fig. 1a and b in comparison), which could sequester the MLD from the NCD. Meanwhile, the C-terminal end of the MLD is linked to the interdomain linker stretch involving β10 and β11, which make frequent contact with the N-terminal stretch including the β1 and α1. The present results showed that defects in the N-terminal stretch (β1 and α1), which could unchain the interdomain linker stretch, resulted in the unfolding of the MLD (Fig. 2f). Thus, the attachment of the interdomain linker stretch to the N-terminal stretch appears to be the critical factor stabilizing the MLD fold, by locating the MLD to be packed onto the NCD. Then, for activation, the stabilizing elements in the inactive ^{R}Hsp33^{M} should also be able to sense and respond to oxidative and thermal stressors. In this context, the zinc binding coordinated solely by the cysteines would be the most effective way to facilitate redox sensing. The tightly bound zinc can be easily released by the oxidation of the cysteines to induce the rapid unfolding of the CRD [8]. However, as depicted in the ^{hO}Hsp33^{M} conformation, unfolding of the CRD is not directly connected with the MLD unfolding (Fig. 2b). The MLD-stabilizing element would therefore require a different path of regulation, presumably by heat. This postulation is supported by the fact that the oxidation of Hsp33 at low temperatures results in the predominant formation of ^{hO}Hsp33^{M}, wherein the CRD is unfolded, but the MLD is not [11]. The presence of a thermal sensing module, independent of the redox-sensing module, is also inferred from the thermal regulation of the cysteine-free form and the CRD-truncated mutants that cannot bind zinc [11,23,30]. Additionally, the M172S mutant of Hsp33 can be activated solely by heat, without oxidation [30]. The present results suggest that the interactions between the interdomain linker stretch and the N-terminal stretch are dynamically organized to easily sense and respond to heat signals. The plausible dynamic fluctuations in those regions could be a thermodynamically favorable feature to rapidly overcome the energy barrier for conformational rearrangement. Winter *et al.* also assumed that the interdomain linker stretch in the ^{hO}Hsp33^{M} state would exist under a dynamic conformational equilibrium [3], undergoing a folding–unfolding exchange for discriminative responses to oxidants with different reaction rates [2,3]. The present results constitute the first experimental evidence that supports the dynamic properties, newly pointing to the N-terminal elements, in addition to the linker stretch, as the dynamic regions. Furthermore, our results indicate that such peculiar dynamics do not begin at the ^{hO}Hsp33^{M} state but rather already occur in the reduced, inactive state (^{R}Hsp33^{M}), allowing for more efficient heat sensing and a rapid onset of structural conversion.

It is noted again that the chaperone function of Hsp33 is achieved by a response to the dual stresses of oxidation and heat [11]. The present structural insight suggests that the dynamic interaction between the interdomain linker stretch and the N-terminal stretch functions as a heat-sensing module, while the zinc coordination functions as a redox-sensing module. Accordingly, the activation process of Hsp33 should be driven by a disruption of the regulatory modules. Among them, the release of the interdomain linker stretch from the N-terminal stretch, rather than the dissociation of zinc, appears to be a more critical factor for conferring chaperone activity, as the active mutants in the present study maintained the folded CRD. This statement is also supported by the fact that the unfolded MLD including the interdomain linker stretch, but not the unfolded CRD, is involved in the substrate-binding sites of the activated Hsp33 [19]. However, it is also possible to presume that the two regulatory units are coupled to provide modulative reactions. For instance, the oxidation of Hsp33 by the kinetically fast oxidant, the hypochlorite ion, can activate the protein without a thermal stressor, whereas oxidation by the kinetically slow oxidant, the peroxide ion, requires heat shock to fully activate the protein [2,3]. The different oxidation results were attributed to the disulfide bond formation between C232 and C234, which can be achieved by the hypochlorite ion at a normal temperature but not by the peroxide ion [2,3]. The residues C232 and C234 are directly connected to the interdomain linker stretch and are located nearby the N-terminal stretch (Fig. 1). The present NMR spectra implied that the six-residue N-terminal deletion likely changed the dynamic properties of the linker stretch. Likewise, it would be reasonable to postulate that the linker dynamics and/or conformation can also be modulated by the formation of the C232–C234 disulfide bond, thereby depriving the linker stretch of its heat-sensing role. Thus, upon formation of the C232–C234 disulfide bond, the MLD could undergo unfolding even at normal temperature, as the linker stretch could not be stringed to the N-terminal stretch. Similarly, the incomplete activity of ^{hO}Hsp33^{M} and ΔC-Hsp33^{D}, which are not reactive to the fast denaturation of substrates [11], is attributable to the maintained linker dynamics due to the absence of the C232–C234 disulfide bond, even with the unfolding or truncation of the CRD.

The dimerization and/or oligomerization of Hsp33 have been suggested to enhance its potency as a holdase [13,15], although it is not critical for obtaining chaperone activity [9,10,14,30]. However, the structural principle of molecular association has been one of the most inexplicable issues in the characterization of the Hsp33 activation process [12]. In the present results, both the β1/α1-defective mutant,

which retained the folded CRD with an intrinsically unfolded linker stretch in the MLD, and the wild-type ^{hO}Hsp33^{M}, where the CRD was unfolded with the retention of β1/α1–β10/β11 interactions, exclusively adopted monomeric states. Thus, the aforementioned coupling of the two regulatory modules (thermal and redox) appears to be important for the molecular association of Hsp33 during its activation process. In addition, it is worthy of notice that the NMR signals from the E150 residue were detectable at a high temperature but not at a normal temperature (Fig. 3), implying dynamic behavior of the residue. Mutation at E150 impairs the dimerization of Hsp33, as the S149–Q151 region constitutes the most critical dimeric interface [9,22]. Thus, this result may suggest that the dimerization of Hsp33 is also under the regulation of dynamic properties that depend on the oxidative and/or thermal status. In conclusion, the present results suggest that the dynamic interactions between the N-terminal stretch and the interdomain linker stretch are the most critical factor for the regulation of the functional activation of Hsp33. Hence, a detailed analysis of molecular dynamics is required to achieve a comprehensive understanding of the activation process of post-translationally regulated chaperones.

Materials and Methods

Protein preparations

Preparation of wild-type Hsp33 in a reduced form and the preparation of isotope-enriched NMR samples were performed according to the previously described methods [12,24,33]. Details of the mutant protein preparations can be found in Supplementary Methods. Briefly, using the pUJ30 (pET11a-*hslO*) [1] plasmid as a template, the ΔN^{6}-, ΔN^{9}-, ΔN^{12}-, and ΔN^{15}-Hsp33 mutants were subcloned into the pET21a vector (Novagen), and the L30K- and Y12E-Hsp33 mutants were generated by introducing single-site mutations into the wild-type Hsp33 gene (*hslO*). The constructed plasmids containing the mutant forms were transformed into the *Escherichia coli* JH13 (BL21, Δ*hslO*) [1] strain. The protocol for wild-type Hsp33 was followed for the purification and oxidation of the mutant proteins, which were expressed at 15 °C.

NMR spectroscopy

NMR samples contained approximately 0.6 mM proteins in the standard buffer (25 mM Tris–HCl containing 50 mM NaCl at pH 7.4). For reduced forms, the solution contained an additional 5 mM dithiothreitol and 20 μM $ZnSO_4$. The sample pH was finely adjusted to 7.4 or 6.5 with the addition of 0.1 N HCl prior to the NMR measurement. All NMR spectra were measured on a Bruker Biospin Avance 900 spectrometer equipped with a cryoprobe, at 298 K and 313 K, respectively. Conventional 2D [^{1}H/^{15}N]TROSY, a series of TROSY-based triple-resonance spectra {HNCACB, HN(CO)CACB, HNCO, and HN(CA)CO}, and a 3D [^{15}N]edited NOESY (HSQC) (150 ms of mixing time) of the [^{13}C/^{15}N/^{2}H]Hsp33 were acquired for the backbone NMR assignments. Chemical shifts were referenced directly to 4,4-dimethyl-4-silapentane-1-sulfonic acid for ^{1}H and indirectly for the ^{15}N and ^{13}C atoms using the chemical shift ratios suggested in the Biological Magnetic Resonance Bank[†]. The assigned $^{13}C^{\alpha}$ and $^{13}C^{\beta}$ chemical shifts were corrected to account for the deuterium isotope effects [25,34-36], prior to the secondary structure determination using the chemical shift values. For a structural comparison, the 2D [^{1}H/^{15}N]TROSY spectra of the wild-type and mutant Hsp33 proteins were obtained using [^{15}N]enriched samples without deuteration.

3D structure generation

Details of the semi-empirical structure determination and refinement can be found in Supplementary Methods. Briefly, the initial 50 structures were generated by the CSA [29] protocol implemented in the CHARMM program [37], using the distance restraints, dihedral φ and ϕ angle restraints, and multiple homology-derived restraints. The average structure was generated from the selected 20-structure ensemble with the lowest energy, followed by a final refinement via a restrained molecular dynamics simulation in explicit water.

CD spectroscopy

Far-UV CD spectra of the wild-type and mutant Hsp33 species (5–10 μM) were recorded in the standard buffer at 20 °C, using a 0.1-cm-pathlength cell on a Jasco J-710 spectropolarimeter equipped with a temperature controller. Three individual scans taken from 260 nm to 190 nm, with a 0.2-nm step resolution, a 1-nm bandwidth, and a 1-s response time, were summed and averaged, followed by a subtraction of the solvent CD signal. Finally, the CD intensity at a wavelength λ was normalized as the mean residue molar ellipticity, $[\theta]_{\lambda}$ (deg cm^{2} dmol^{-1}) [38].

Gel-filtration analysis

Purified protein solutions concentrated at around 300 μM (700 μl injection each) were loaded onto a HiLoad 16/60 Superdex™ 75 (GE Healthcare) column pre-equilibrated with the standard buffer. The protein was eluted at a flow rate of 1 ml/min and was detected by measuring the absorbance of the eluates at 280 nm. The hydrodynamic size was represented by the apparent molecular mass (M_r^{app}, kDa), which was deduced from the elution volume, as previously described [12].

MALS analysis

Purified protein solutions were loaded onto a size-exclusion chromatography column (WTC-015S5; Wyatt Technologies) that was connected with a MALS detector

(DAWN HELEOS-II; Wyatt Technologies) and a differential refractive index detector (Optilab T-rEX; Wyatt Technologies). The column was pre-equilibrated with the standard buffer at a flow rate of 0.5 ml/min. The weight averaged molar masses were calculated from the elution data, using the ASTRA software (Wyatt Technologies).

Chaperone activity assay

Chaperone activity was assessed by monitoring the effect of the wild-type and mutant Hsp33 species on the aggregation of an experimental client protein, CS. For the thermal aggregation assay [1,3,13], reaction buffer (40 mM Hepes–KOH at pH 7.5) alone or with 0.45 μM Hsp33 was pre-incubated at 43 °C for 1 min, followed by the addition of CS to a final concentration of 0.1 μM. The kinetic trace of light scattering from the aggregated CS was recorded at 360 nm, with a 5-nm slit width for excitation and emission on a Varian Cary Eclipse spectrofluorophotometer, with continuous stirring. For the chemical aggregation assay [1,9–11,30], 12 μM CS was denatured in the reaction buffer containing 4.5 M GdnHCl for 90 min at room temperature. Protein aggregation was initiated by diluting the denatured CS to a final concentration of 75 nM (160-fold dilution) into the reaction buffer without GdnHCl at 30 °C under constant stirring. To test the activity of Hsp33 species, we supplemented the buffer with an Hsp33 species at designated concentrations and we monitored light scattering at 360 nm.

Funding

This research was supported by Basic Science Research Program through the National Research Foundation of Korea (NRF) funded by the Ministry of Education, Science and Technology (No. 2010-0006022 and in part 2013R1A1A2007774).

Acknowledgements

We thank Dr. Ursula Jakob (University of Michigan, USA) for generously providing the recombinant plasmid pUJ30 and the *E. coli* JH13 strain. This work made use of the NMR, fluorescence, CD, and MALS machines at the Korea Basic Science Institute (Ochang, Korea). The NMR experiments in particular were supported by a grant from the High-Field NMR Research Program of the Korea Basic Science Institute.

Appendix A. Supplementary data

Supplementary data to this article can be found online at http://dx.doi.org/10.1016/j.jmb.2015.09.029.

Received 30 March 2015;
Received in revised form 21 September 2015;
Accepted 30 September 2015
Available online 8 October 2015

Keywords:
molecular chaperone;
oxidative stress;
redox regulation;
nuclear magnetic resonance;
conformational change

[8]J.L. was supported by the Korean Research Institute of Bioscience and Biotechnology Research Initiative Program.

[9]Present address: T.-G. Jung, Department of Bio-Engineering, Life Science RD Center, Sinil Pharmaceutical Co., Gyeonggi 13207, Republic of Korea.

†http://www.bmrb.wisc.edu.

Abbreviations used:
CRD, C-terminal regulatory domain; CS, citrate synthase; CSA, conformational space annealing; Hsp33, heat shock protein 33; HSQC, heteronuclear single quantum coherence; MALS, multi-angle light scattering; MLD, middle linker domain; NCD, N-terminal core domain; NOE, nuclear Overhauser enhancement; NOESY, NOE spectroscopy; TROSY, transverse relaxation optimized spectroscopy.

References

[1] U. Jakob, W. Muse, M. Eser, J.C.A. Bardwell, Chaperone activity with a redox switch, Cell 96 (1999) 341–352.
[2] C. Kumsta, U. Jakob, Redox-regulated chaperones, Biochemistry 48 (2009) 4666–4676.
[3] J. Winter, M. Ilbert, P.C. Graf, D. Ozcelik, U. Jakob, Bleach activates a redox-regulated chaperone by oxidative protein unfolding, Cell 135 (2008) 691–701.
[4] W.Y. Wholey, U. Jakob, Hsp33 confers bleach resistance by protecting elongation factor Tu against oxidative degradation in *Vibrio cholerae*, Mol. Microbiol. 83 (2012) 981–991.
[5] H.-J. Kang, D.-H. Heo, S.-W. Choi, K.-N. Kim, J. Shim, C.-W. Kim, et al., Functional characterization of Hsp33 protein from *Bacillus psychrosaccharolyticus*; additional function of HSP33 on resistance to solvent stress, Biochem. Biophys. Res. Commun. 358 (2007) 743–750.
[6] M.L. Evans, J.C. Schmidt, M. Ilbert, S.M. Doyle, S. Quan, J.C.A. Bardwell, et al., *E. coli* chaperones DnaK, Hsp33 and Spy inhibit bacterial functional amyloid assembly, Prion 5 (2011) 323–334.
[7] N. Bruel, M.-P. Castanié-Cornet, A.-M. Cirinesi, G. Koningstein, C. Georgopoulos, J. Luirink, et al., Hsp33 controls elongation factor-Tu stability and allows *Escherichia coli* growth in the absence of the major DnaK and trigger factor chaperones, J. Biol. Chem. 287 (2012) 44435–44446.
[8] H.-S. Won, L.Y. Low, R.D. Guzman, M. Martinez-Yamout, U. Jakob, H.J. Dyson, The zinc-dependent redox switch domain of the chaperone Hsp33 has a novel fold, J. Mol. Biol. 341 (2004) 893–899.

[9] P.C. Graf, M. Martinez-Yamout, S. VanHaerents, H. Lilie, H.J. Dyson, U. Jakob, Activation of the redox-regulated chaperone Hsp33 by domain unfolding, J. Biol. Chem. 279 (2004) 20529–20538.
[10] S. Barbirz, U. Jakob, M.O. Glocker, Mass spectrometry unravels disulfide bond formation as the mechanism that activates a molecular chaperone, J. Biol. Chem. 275 (2000) 18759–18766.
[11] M. Ilbert, J. Horst, S. Ahrens, J. Winter, P.C. Graf, H. Lilie, et al., The redox-switch domain of Hsp33 functions as dual stress sensor, Nat. Struct. Mol. Biol. 14 (2007) 556–563.
[12] Y.-S. Lee, K.-S. Ryu, S.-J. Kim, H.-S. Ko, D.-W. Sim, Y.H. Jeon, et al., Verification of the interdomain contact site in the inactive monomer, and the domain-swapped fold in the active dimer of Hsp33 in solution, FEBS Lett. 586 (2012) 411–415.
[13] M.W. Akhtar, V. Srinivas, B. Raman, T. Ramakrishna, T. Inobe, K. Maki, et al., Oligomeric Hsp33 with enhanced chaperone activity: Gel filtration, cross-linking, and small angle X-ray scattering (SAXS) analysis, J. Biol. Chem. 279 (2004) 55760–55769.
[14] S.-W. Chi, D.G. Jeong, J.R. Woo, H.S. Lee, B.C. Park, B.Y. Kim, et al., Crystal structure of constitutively monomeric *E. coli* Hsp33 mutant with chaperone activity, FEBS Lett. 585 (2011) 664–670.
[15] J. Graumann, H. Lilie, T. Xianli, K.A. Tucker, J.H. Hoffmann, J. Vijayalakshmi, et al., Activation of the redox-regulated molecular chaperone Hsp33—A two-step mechanism, Structure 9 (2001) 377–387.
[16] J.H. Hoffmann, K. Linke, P.C. Graf, H. Lilie, U. Jakob, Identification of a redox-regulated chaperone network, EMBO J. 23 (2004) 160–168.
[17] I. Janda, Y. Devedjiev, U. Derewenda, Z. Dauter, J. Bielnicki, D.R. Cooper, et al., The crystal structure of the reduced, Zn^{2+}-bound form of the *B. subtilis* Hsp33 chaperone and its implications for the activation mechanism, Structure 12 (2004) 1901–1907.
[18] M.P. Mayer, The unfolding story of a redox chaperone, Cell 148 (2012) 843–844.
[19] D. Reichmann, Y. Xu, C.M. Cremers, M. Ilbert, R. Mittelman, M.C. Fitzgerald, et al., Order out of disorder: Working cycle of an intrinsically unfolded chaperone, Cell 148 (2012) 947–957.
[20] D. Reichmann, U. Jakob, The roles of conditional disorder in redox proteins, Curr. Opin. Struct. Biol. 23 (2013) 436–442.
[21] S.-J. Kim, D.-G. Jeong, S.-W. Chi, J.-S. Lee, S.-E. Ryu, Crystal structure of proteolytic fragments of the redox-sensitive Hsp33 with constitutive chaperone activity, Nat. Struct. Mol. Biol. 8 (2001) 459–466.
[22] J. Vijayalakshmi, M.K. Mukhergee, J. Graumann, U. Jakob, M.A. Saper, The 2.2 Å crystal structure of Hsp33: A heat shock protein with redox-regulated chaperone activity, Structure 9 (2001) 367–375.
[23] L. Jaroszewski, R. Schwarzenbacher, D. McMullan, P. Abdubek, S. Agarwalla, E. Ambing, et al., Crystal structure of Hsp33 chaperone (TM1394) from *Thermotoga maritima* at 2.20 Å resolution, Proteins 61 (2005) 669–673.
[24] Y.-S. Lee, H.-S. Won, Backbone NMR assignments of a prokaryotic molecular chaperone, J. Korean Magn. Reson. Soc. 16 (2012) 172–184.
[25] R.A. Venters, B.T. Farmer 2nd, C.A. Fierke, L.D. Spicer, Characterizing the use of perdeuteration in NMR studies of large proteins: ^{13}C, ^{15}N and ^{1}H assignments of human carbonic anhydrase II, J. Mol. Biol. 264 (1996) 1101–1116.
[29] J. Lee, H.A. Scheraga, S. Rackovsky, New optimization method for conformational energy calculations on polypeptides: Conformational space annealing, J. Comput. Chem. 18 (1997) 1222–1232.
[26] Y. Shen, F. Delaglio, G. Cornilescu, A. Bax, TALOS+: A hybrid method for predicting protein backbone torsion angles from NMR chemical shifts, J. Biomol. NMR 44 (2009) 213–223.
[27] D.S. Wishart, B.D. Sykes, The ^{13}C chemical-shift index: A simple method for the identification of protein secondary structure using ^{13}C chemical-shift data, J. Biomol. NMR 4 (1994) 171–180.
[28] T.-R. Kim, S. Ji, S. Lee, I.-S. Chu, S. Shin, J. Lee, A hybrid modeling strategy using nuclear Overhauser effect data with contact information, Chem. Phys. Lett. 554 (2012) 190–194.
[30] C.M. Cremers, D. Reichmann, J. Hausmann, M. Ilbert, U. Jakob, Unfolding of metastable linker region is at the core of Hsp33 activation as a redox-regulated chaperone, J. Biol. Chem. 285 (2010) 11243–11251.
[31] B. Raman, S. Kumar, T. Ramakrishna, C.M. Rao, Redox-regulated chaperone function and conformational changes of *Escherichia coli* Hsp33, FEBS Lett. 489 (2001) 19–24.
[32] U. Jakob, M. Eser, J.C.A. Bardwell, Redox switch of hsp33 has a novel zinc-binding motif, J. Biol. Chem. 275 (2000) 38302–38310.
[33] Y.-S. Lee, H.-S. Ko, K.-S. Ryu, Y.-H. Jeon, H.-S. Won, Triple isotope-[^{13}C, ^{15}N, ^{2}H] labeling and NMR measurements of the inactive, reduced monomer form of *Escherichia coli* Hsp33, J. Korean Magn. Reson. Soc. 14 (2010) 117–126.
[34] K.H. Gardner, L.E. Kay, The use of ^{2}H, ^{13}C, ^{15}N multidimensional NMR to study the structure and dynamics of proteins, Annu. Rev. Biophys. Biomol. Struct. 27 (1998) 357–406.
[35] X. Shan, K.H. Gardner, D.R. Muhandiram, L.E. Kay, C.H. Arrowsmith, Subunit-specific backbone NMR assignments of a 64 kDa trp repressor/DNA complex: A role for N-terminal residues in tandem binding, J. Biomol. NMR 11 (1998) 307–318.
[36] H.-S. Won, T. Yamazaki, T.-W. Lee, M.-K. Yoon, S.-H. Park, Y. Kyogoku, et al., Structural understanding of the allosteric conformational change of cyclic AMP receptor protein by cyclic AMP binding, Biochemistry 39 (2000) 13953–13962.
[37] B.R. Brooks, C.L. Brooks 3rd, A.D. Mackerell Jr., L. Nilsson, R.J. Petrella, B. Roux, et al., CHARMM: The biomolecular simulation program, J. Comput. Chem. 30 (2009) 1545–1614.
[38] H.-S. Won, S.-H. Park, H.E. Kim, B. Hyun, M. Kim, B.J. Lee, et al., Effects of a tryptophanyl substitution on the structure and antimicrobial activity of C-terminally truncated gaegurin 4, Eur. J. Biochem. 269 (2002) 4367–4374.
[39] E.F. Pettersen, T.D. Goddard, C.C. Huang, G.S. Couch, D.M. Greenblatt, E.C. Meng, et al., UCSF Chimera—A visualization system for exploratory research and analysis, J. Comput. Chem. 25 (2004) 1605–1612.